

Structural, magnetic and electrical properties of single crystalline $\text{La}_{1-x}\text{Sr}_x\text{MnO}_3$ for $0.4 < x < 0.85$

J. Hemberger¹, A. Krimmel¹, T. Kurz¹, H.-A. Krug von Nidda¹,
 V.Yu. Ivanov², A.A. Mukhin², A.M. Balbashov³, A. Loidl¹
¹*Experimentalphysik V, Elektronische Korrelationen und Magnetismus,*
Institut für Physik, Universität Augsburg, D-86135 Augsburg, Germany

²*General Physics Institute of the Russian Academy of Sciences, 38 Vavilov St., 117942 Moscow, Russia*

³*Moscow Power Engineering Institute, 14 Krasnokazarmennaya St., 105835 Moscow, Russia*

We report on structural, magnetic and electrical properties of Sr-doped LaMnO_3 single crystals for doping levels $0.4 \leq x \leq 0.85$. The complex structural and magnetic phase diagram can only be explained assuming significant contributions from the orbital degrees of freedom. Close to $x = 0.6$ a ferromagnetic metal is followed by an antiferromagnetic metallic phase below 200 K. This antiferromagnetic metallic phase exists in a monoclinic crystallographic structure. Following theoretical predictions this metallic antiferromagnet is expected to reveal an (x^2-y^2) -type orbital order. For higher Sr concentrations an antiferromagnetic insulator is established below room temperature.

PACS numbers: 75.30.-m, 77.30.Kg, 72.80.Ga

I. INTRODUCTION

The fascinating phase diagrams of the doped manganites result from a subtle interplay of spin, charge, orbital and lattice degrees of freedom. In $\text{La}_{1-x}\text{Sr}_x\text{MnO}_3$ the main body of experimental investigations has been carried out for Sr concentrations $x < 0.5$. This partly has been due to the fact that colossal magnetoresistance effects¹ show up around $x = 0.3$, which in the beginning of the research seemed to be rather promising for application. On the other hand single crystals for $x > 0.5$ are hard to grow and hence, only rarely have been investigated.

Already at low concentrations ($x < 0.5$) a rather complex phase diagram evolves, which is due to the fact that in addition to super-exchange (SE) and double-exchange (DE) interactions, charge order (CO) and structural effects via orbital ordering are of outstanding importance. For $x < 0.2$, a long-range cooperative Jahn-Teller (JT) effect establishes orbital order (OO), which finally determines the antiferromagnetic (AFM) spin state of A-type in the pure compound at low temperatures. With increasing Sr doping ($x < 0.1$) a ferromagnetic (FM) component evolves in addition to the AFM order of subsequent planes which is explained in terms of electronic phase separation² or, following the time-honored ideas of de Gennes³, in terms of a canted AFM (CA) state. However, within this model of competing SE and DE interactions clearly the importance of lattice distortions has to be taken into account.⁴ On further increasing x ($0.1 \leq x \leq 0.17$), it seems clear that a new type of orbital order, probably connected with CO, determines the low-temperature insulating ferromagnet (FM) around $x = 0.125$.^{5,6,7} Finally, for Sr concentrations $x > 0.17$ the long-range JT distortions become suppressed and a ferromagnetic metal evolves below the FM phase transition which is stable almost up to half filling.

After the early work on La:SrMnO_3 which is summa-

rized by Goodenough and Longo⁸, the complex phase diagram has been studied by many groups and a more or less coherent picture can be deduced from the variety of experimental results reported.^{6,9,10,11,12} From the systems with narrower bandwidth (e.g. $L_{1-x}A_x\text{MnO}_3$ with $L = \text{Nd, Pr, Sm}$ and $A = \text{Ca, Sr}$ ^{13,14}) an extreme asymmetry between the hole and electron doped regimes is well known and it seems highly interesting also to investigate the electron doped $\text{La}_{1-x}\text{Sr}_x\text{MnO}_3$. However, for $x > 0.5$ much less experimental information is available.

Structural, resistivity and magnetization results for $x = 0.5$ and 0.54 were reported by Akimoto et al.¹⁵ For $x = 0.54$ they reported an orthorhombic ($Pbnm$) nuclear and an A-type AFM structure at 10 K. Results for similar Sr concentrations $0.5 < x < 0.6$ were published by Moritomo et al.¹⁶ On increasing x , the crystal symmetry changes from rhombohedral ($R3c$) to pseudotetragonal at $x = 0.54$ with $a \approx b < c\sqrt{2}$. For concentrations around $x = 0.55$, a metallic AFM phase, with A-type spin structure at low temperatures, is followed by a FM metallic (M) state at elevated temperatures.¹⁶ Polycrystalline $\text{La}_{1-x}\text{Sr}_x\text{MnO}_3$ has been investigated by Fujishiro et al.¹⁷ by magnetization, electrical resistivity and ultrasonic techniques. They arrive at a different phase diagram, with an insulating (I) state for all concentrations $x > 0.5$. Similar findings were reported by Patil et al.¹⁸ who also investigated ceramic samples for $0.46 \leq x \leq 0.53$. They found a sequence of magnetic and charge-order transitions and interpreted their results in terms of electronic phase separation.

Further interest in the overdoped manganites arises from the fact that for the insulating regions of the phase diagram electronic phase separation in form of stripes²⁰ or bistripes²¹ has been reported. This special form of CO certainly is driven by OO.²² Also theoretically the phase diagrams of the doped manganites have been investigated in great detail.^{2,13,22,23,24} Specifically in Ref.²⁴ the overdoped regime was investigated using DE within

degenerate orbitals. Depending on the bandwidth, on increasing electron doping a sequence of spin structures of type A, C, A and F has been predicted.^{24,25}

In order to clarify the situation and to shed some light on the complex and complete (x, T) -phase diagram in $\text{La}_{1-x}\text{Sr}_x\text{MnO}_3$ we grew a series of single crystals for concentrations $(0.4 < x < 0.85)$. We were not able to grow crystals with higher Sr concentrations. The reason seems to be rather clear as SrMnO_3 reveals a hexagonal crystal structure and obviously there exists a miscibility gap for concentrations close to pure SrMnO_3 . In the following we present detailed structural, magnetic susceptibility, magnetization and electrical resistivity results for the complete series of crystals. From the results we construct a detailed phase diagram. Polycrystalline SrMnO_3 has been investigated to complete the phase diagram. These experiments are a continuation of earlier work on crystals with low Sr doping levels which has been published previously⁶ and has been included to present the complete (x, T) -phase diagram of $\text{La}_{1-x}\text{Sr}_x\text{MnO}_3$ for $0 \leq x \leq 1$.

II. EXPERIMENTAL DETAILS

$\text{La}_{1-x}\text{Sr}_x\text{MnO}_3$ single crystals were grown by a floating-zone method with radiation heating similar to the techniques as described in Ref.²⁶ For these crystals with Sr concentrations $x \geq 0.5$, different atmospheric conditions ranging from air atmosphere to excess oxygen pressure up to 50 atm were tested to optimize the growth process. Nevertheless an uncertainty in the control of the concentration x of up to 2% cannot be ruled out. To complement the phase diagram pure SrMnO_3 has been grown using standard ceramic techniques. Powder x-ray diffraction measurements were performed utilizing $\text{Cu-K}\alpha$ radiation with $\lambda = 0.1541$ nm.

The magnetic susceptibility and magnetization were measured using a commercial superconducting quantum interference device (SQUID) magnetometer ($1.5 < T < 400$ K, $H \leq 50$ kOe) and an ac-magnetometer which operates up to magnetic fields of $H = 140$ kOe. The electrical resistance has been measured using standard four-probe techniques in home-built cryostats and ovens from 1.5 K to 600 K.

III. RESULTS AND DISCUSSION

A. X-ray diffraction

To demonstrate the quality of the single crystals under investigation, we powdered pieces of the single crystals used for magnetic and transport measurements and performed detailed Rietveld refinements of the diffraction profiles for samples with Sr concentrations $0.55 \leq x \leq 0.85$ at room temperature. Fig. 1 shows the diffraction profiles, the refinement and the difference pattern for

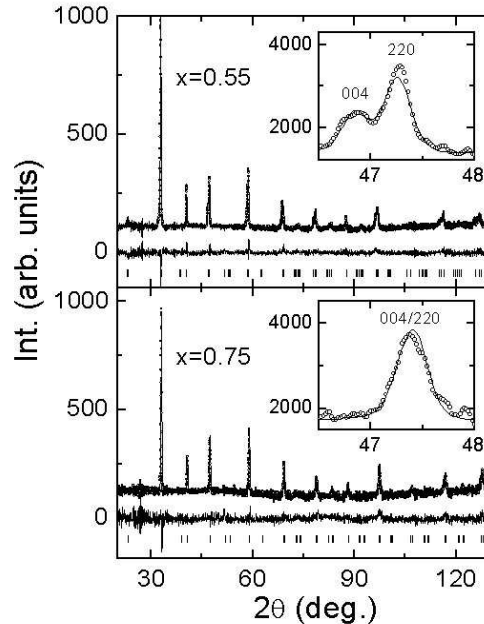


FIG. 1: X-ray diffraction profiles of $\text{La}_{1-x}\text{Sr}_x\text{MnO}_3$ for concentrations $x = 0.55$ (upper frame) and $x = 0.75$ (lower frame). The solid lines correspond to the results of a Rietveld refinement. The difference patterns are indicated in each frame. The insets show the splitting of the [220] and [004] reflexes, denoting the decrease of the tetragonal distortion with increasing x .

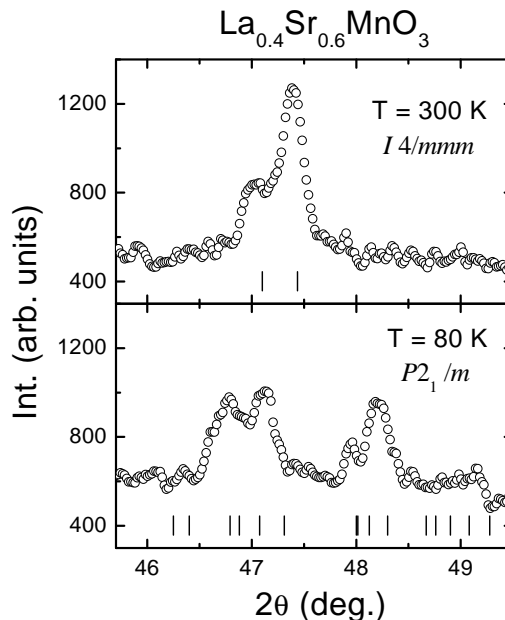


FIG. 2: Parts of the temperature dependent x-ray powder diffraction patterns of $\text{La}_{0.4}\text{Sr}_{0.6}\text{MnO}_3$ for $46^\circ < 2\theta < 49^\circ$. At $T = 80$ K pronounced superlattice reflections around $2\theta \approx 48^\circ$ indicate a monoclinic distortion.

TABLE I: Room temperature crystal symmetry and lattice parameters of $\text{La}_{1-x}\text{Sr}_x\text{MnO}_3$ for Sr-concentrations ($0.5 \leq x \leq 1.0$). The diffraction data for $x < 1$ were derived from single crystalline material which was powdered for the diffraction measurements. The two lowest rows display Curie-Weiss temperatures T_{CW} and the effective paramagnetic moments μ_{eff} obtained from the linear regime of the inverse susceptibility below $T = 400$ K.

x	0.5	0.55	0.6	0.65	0.75	0.85	1.0
crystal structure	rhombohedral	tetragonal	tetragonal	tetragonal	tetragonal	tetragonal	hexagonal
a [Å]	5.461	5.438	5.448	5.437	5.419	5.404	5.452
c [Å]	-	7.753	7.672	7.670	7.686	7.665	9.084
$c/\sqrt{2}a$	-	1.008	0.996	0.997	1.002	1.003	-
α [°]	60.16						
T_{CW} [K]	333	313	299	255	64	-2	-980
μ_{eff} [μ_B]	5.1	5.0	4.9	4.8	4.9	4.6	4.0

$x = 0.55$ (upper panel) and $x = 0.75$ (lower panel). First of all we want to stress that all reflections can be indexed and no impurity phases are apparent above the background level, even no spurious amount of SrMnO_3 which has been reported in all previous investigations.^{8,15,16,17} At first sight one recognizes that with increasing Sr concentration x the crystals almost approach cubic symmetry which is expected for concentrations with a tolerance factor close to 1. This is demonstrated by the insets in Fig. 1, showing the splitting of the 220/004 reflections which provides direct experimental evidence of the c/a ratio and hence on the tetragonal distortion. For $x = 0.55$ a clear splitting of the reflections can be detected, while for $x = 0.75$ no apparent splitting is visible and a splitting can only be derived via the broadening of the reflection in a detailed Rietveld refinement with well defined resolution parameters. Hence the samples near $x = 0.8$ are very close to cubic symmetry.

From the Rietfeld refinement we determined the lattice constants of the samples under investigation. The results are listed in Tab. 1. At room temperature the structure changes from rhombohedral (R) at $x = 0.5$ to tetragonal (T) at $x = 0.55$ and finally to hexagonal (H) close to pure SrMnO_3 . We would like to recall that SrMnO_3 was only prepared in ceramic form and we were not able to grow crystals beyond strontium concentrations $x = 0.85$. The room-temperature tetragonal phase extends over a broad concentration range, with a significant change of the tetragonal distortion. For $x = 0.55$ we find a value of $c/\sqrt{2}a \approx 1.01$. Note that for this concentration ferromagnetism is established already at room temperature. On increasing x this ratio is reduced yielding values close to 1, however now in the paramagnetic phase, but still on the verge of magnetic order. It is clear that the c/a ratio will strongly depend on the orbital structure, i.e. whether the orbitals are aligned as $d_{x^2-y^2}$ or as $d_{3z^2-r^2}$. However, systematic temperature dependent x-ray diffraction measurements are needed to arrive at final conclusions. From preliminary temperature-dependent x-ray diffraction experiments (down to 80 K) we found that for $0.5 < x < 0.7$ the symmetry is lowered and the structure changes into a monoclinic (Mc)

phase characterized by space group $P2_1/m$. Fig. 2 illustrates the evolution of superlattice reflections for $x = 0.6$ due to the monoclinic distortion on cooling. At the boundaries of this monoclinic low-temperature phase for $x \approx 0.5$ and $x \approx 0.7$ we suggest that the system enters into a structurally mixed phase where the Mc phase coexists with a R and T phase, respectively. However a more detailed evaluation is necessary to analyze these two-phase regions. A detailed report on the structural properties will be given elsewhere.²⁷ It should be noticed that a low-temperature monoclinic phase with space group $P2_1/m$ has been established in the doped manganites $\text{La}_{0.5}\text{Ca}_{0.5}\text{MnO}_3$ and $\text{Pr}_{0.6}(\text{Ca}_{1-x}\text{Sr}_x)_{0.4}\text{MnO}_3$, as well as in $\text{Pr}_{0.5}\text{Sr}_{0.5}\text{MnO}_3$.^{28,29,30} Furthermore, the presence of monoclinic domains within an orthorhombic matrix has been reported for $\text{Pr}_{0.7}\text{Ca}_{0.25}\text{Sr}_{0.05}\text{MnO}_3$ and $\text{Pr}_{0.75}\text{Sr}_{0.25}\text{MnO}_3$ on the basis of high-resolution microscopy.³¹

B. Transport properties

Fig. 3 shows the temperature dependence of the electrical resistivity below room temperature. Clearly $\text{La}_{1-x}\text{Sr}_x\text{MnO}_3$ reveals a metallic conductivity for $0.4 < x < 0.6$. These findings differ from those reported by Patil et al.¹⁸ for concentrations close to $x = 0.5$ obtained from ceramic samples, where the resistivity increases towards low temperatures. From optical measurements these authors find indications for an anisotropy of the conductivity. This fact together with possible grain effects in ceramic samples could explain the different results.

For Sr concentrations $x = 0.625$ and 0.7 a significant increase of the resistivity occurs below 250 K. Finally in the samples with $x > 0.7$ this feature is sharper and denotes the transition from the paramagnetic to the anti-ferromagnetic state. Towards low temperatures a purely semiconducting behavior can be found. It seems that the samples with Sr concentration $x \approx 0.7$ belong to a two-phase region separating metallic and insulating regimes. At the same time the system is close to a phase boundary

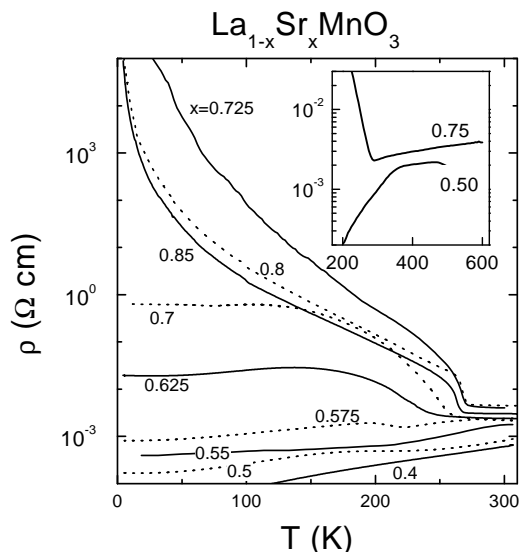


FIG. 3: Temperature dependence of the resistivity in $\text{La}_{1-x}\text{Sr}_x\text{MnO}_3$ for different concentrations $0.4 \leq x \leq 0.85$ as indicated in the figure. The inset shows the resistivity for $x = 0.5$ and $x = 0.75$ measured also at higher temperatures.

between the monoclinic and tetragonal crystal structures. Nevertheless, the sample with $x = 0.7$ remains a candidate for the occurrence of electronic phase separation for $T < 200$ K. To investigate also the high-temperature electronic behavior, we measured the electrical resistance for some representative samples up to 600 K. The results for $x = 0.5$ and 0.75 are shown in the inset. For $x = 0.5$ the metallic behavior at low temperatures changes into the temperature characteristics of a bad metal at elevated temperatures. For $x > 0.7$ a bad metallic behavior for $T > 250$ K changes into strongly semiconducting temperature characteristics below. The low-temperature resistivity as a function of Sr concentration exhibits a maximum around $x \approx 0.75$. This may indicate a CO state at electronic quarter filling of the e_g bands.

C. Magnetization and magnetic susceptibility

The magnetic dc-susceptibility (M/H measured at 1 kOe) of $\text{La}_{1-x}\text{Sr}_x\text{MnO}_3$ is shown in Fig. 4 in the upper frame. For $x = 0.4$, at 370 K we find the pure ferromagnetic phase transition, which is driven by DE interactions and is characteristic for the materials showing a colossal magneto-resistance (CMR) effect. For $x = 0.5$ and 0.6 the magnetization decreases below 250 K indicating that the ferromagnetic moments become reduced at low temperatures. This may be due to a slight canting of the spins or due to electronic phase-separation effects. Similar findings for $0.46 \leq x \leq 0.53$ were interpreted in terms of phase separation within a charge ordered state.¹⁸ We would like to recall that for $x \approx 0.5$ we found indications of a two-phase region of a rhombohedral and a monoclinic

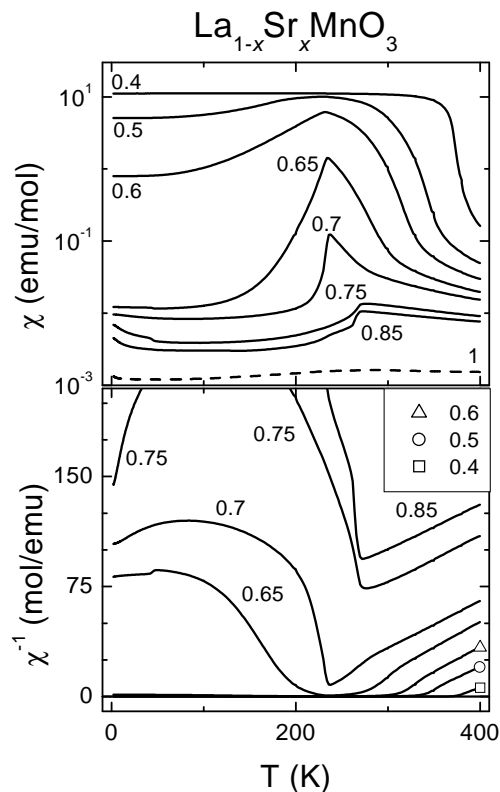


FIG. 4: Temperature dependence of the magnetic susceptibility in $\text{La}_{1-x}\text{Sr}_x\text{MnO}_3$ as measured at a dc magnetic field of 1 kOe, for Sr concentrations from 0.4 to 0.85. In the upper frame the susceptibility is shown as a function of temperature. The lower frame shows the inverse susceptibilities vs. T .

structure. At the moment it is unclear, whether this is a structural two-phase region, or whether the groundstate can be explained in terms of electronic phase separation between FM and AFM regions including scenarios like stripe or bistrife formation.

Well defined cusps appear for $x = 0.65$ and 0.7 which indicate the vanishing of a spontaneous ferromagnetic moment and the presence of a nearly completely antiferromagnetic (AFM) spin-structure at low temperatures. It is important to note that we observed a pronounced temperature hysteresis at these cusps typical for a first-order magnetic transition. Finally for $x > 0.7$ the characteristics of purely antiferromagnetic phase transitions are detected. From the inverse susceptibilities, which are shown in the lower frame of Fig. 4, we can deduce the Curie-Weiss (CW) temperatures, which continuously decrease while the Sr concentration increases from $x = 0.4$ to $x = 0.7$ (cf. Tab. 1). Beyond this concentration a significant decrease of the CW temperatures appears and finally, for $x = 0.85$, a negative CW temperature can be read off. For the concentrations $0.55 \leq x \leq 0.7$ in addition a distinct deviation from the CW behavior can be

detected well above the magnetic ordering temperature indicating the presence of strong spin fluctuations or even of short-range magnetic order.

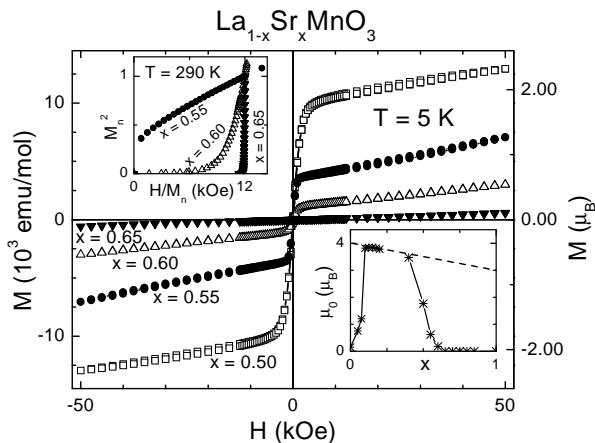


FIG. 5: Low-temperature ($T = 5$ K) magnetization of $\text{La}_{1-x}\text{Sr}_x\text{MnO}_3$ as a function of magnetic field for concentrations $x = 0.5, 0.55, 0.6$ and 0.65 . The lower right inset shows the remnant (ferromagnetic) saturated moment as a function of concentration. The dashed line indicates the saturated moment assuming that all Mn ions (Mn^{3+} and Mn^{4+}) contribute only with their spin values to the ordered moment. The upper left inset shows the normalized magnetization at 290 K for concentrations $x = 0.5, 0.55$, and 0.6 presented as M_n^2 vs. H/M_n with $M_n = M/M(12\text{kOe})$.

To further elucidate the low-temperature magnetic properties of $\text{La}_{1-x}\text{Sr}_x\text{MnO}_3$, Fig. 5 shows the magnetization at 5 K for a series of crystals with concentrations $0.5 < x < 0.65$. An almost pure antiferromagnet at $x = 0.65$ is followed by an increasing ferromagnetic component on decreasing x . But even at $x = 0.5$ only 2/3 of the full possible ferromagnetic magnetization is observed at low fields, and on increasing external field the magnetization increases strictly linearly, which can be explained in terms of a canted antiferromagnet, whose canting angle becomes reduced in increasing fields, or in terms of electronic phase separation. Including earlier published results⁶, the lower inset of Fig. 5 demonstrates, how the ferromagnetic moment evolves in the complete concentration regime. The expected spin-only FM moment only evolves for Sr concentrations $0.2 < x < 0.4$ and approaches values close to zero for lower and higher Sr concentrations. The upper inset of Fig. 5 compares the field dependence of the magnetization for the concentrations $x = 0.55, 0.6$, and 0.65 at $T = 290$ K. The representation M_n^2 vs. H/M_n (Arrot-plot¹⁹) demonstrates the presence of a spontaneous FM component (i.e. finite M^2 at $H = 0$) for $x = 0.55$. At the same temperature the behavior of $x = 0.65$ is purely paramagnetic (i.e. H/M is constant). The curve for $x = 0.6$ exhibits an intermediate behavior, denoting the presence of strong FM fluctuations or short-range order (SR). This corresponds to the strong deviations from the Curie-Weiss behavior

discussed earlier (see Fig. 4).

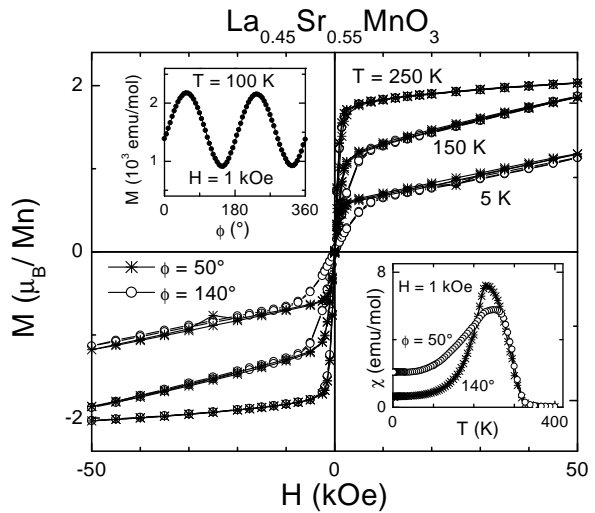


FIG. 6: Magnetization as a function of external field in $\text{La}_{0.45}\text{Sr}_{0.55}\text{MnO}_3$ measured at different temperatures and different orientations with respect to the external field (see upper inset). The solid lines are drawn to guide the eye. The lower inset displays the temperature dependence of the magnetic dc susceptibility $\chi = M/H$, measured at these different orientations.

In what follows, we wanted to study the magnetic anisotropy close to half filling in more detail. Around $x = 0.55$ the ferromagnetic phase at elevated temperatures is followed by a further magnetic phase transition which significantly reduces the magnetization (see Fig. 4). To elucidate the temperature evolution of this weak ferromagnetic regime in more detail, Fig. 6 shows the magnetization vs. external field in $\text{La}_{0.45}\text{Sr}_{0.55}\text{MnO}_3$ for a series of temperatures. At 250 K, just below the FM phase transition a strong ferromagnetic hysteresis evolves and, taking into account the elevated temperature, almost the full saturated moment of $\text{Mn}^{3+}/\text{Mn}^{4+}$ can be detected. However, below 200 K the magnetization at moderate fields becomes significantly reduced and reveals a strictly linear increase of M as function of field. Finally at 5 K the FM component amounts approximately $0.5 \mu_B$ only.

To study the anisotropy of this magnetic ground state, the data were taken for two different orientations of the sample with respect to the external field. The upper inset of Fig. 6 shows the angular dependence of the magnetization as observed at $T = 100$ K when the sample was rotated around an axis approximately within the a, b -plane. From this a hard and an easy axis were defined, which differ by almost a factor of 2.5 in the magnetization values. The lower inset of Fig. 6 shows the temperature dependence of the magnetic susceptibility measured for these both orientations. The distinct evolution of anisotropic behavior below $T \approx 250$ K can be observed. This behavior clearly is different from the anisotropy observed for strontium concentrations of $x = 0.05$ where

IV. CONCLUSION

What did we learn from these experiments in addition to the existing enormous amount of knowledge on the doped manganites? To summarize, we were able to grow high-quality single crystals of $\text{La}_{1-x}\text{Sr}_x\text{MnO}_3$ for $0 \leq x \leq 0.85$ with no parasitic phases like SrMnO_3 . We constructed a rather complete (x, T) phase diagram (Fig. 7), which reveals the well established asymmetry between the hole doped ($x < 0.5$) and the electron doped ($x > 0.5$) regime. Of course, an essential part of this asymmetry is driven by geometrical constraints via the tolerance factor, which increases from $t = 0.89$ for $x = 0$ to $t = 1.01$ for $x = 1$. Hence, on increasing concentration, $\text{La}_{1-x}\text{Sr}_x\text{MnO}_3$ reveals a decreasing buckling of the MnO_6 octahedra. But partly this asymmetry also is driven by orbital degeneracy. Close to $x = 0$ strong JT distortions reveal orbital order which concomitantly determines the A-type spin structure. For higher Sr concentrations and in the crystals with a high symmetry at the Mn site, orbital degeneracy will play an essential role, yielding completely different spin ground states.

In Fig. 7 the combined influence of the concentration dependence of the tolerance factor and the increasing importance of orbital degeneracy as x increases is nicely documented in the sequence of structural phases: At room temperature and for $0 \leq x \leq 0.85$ we find the crystallographic phases O' orthorhombic, O orthorhombic, rhombohedral and tetragonal. The corresponding series of electronic ground-state properties is insulating/spin A-type AFM, insulating/spin FM, metallic/spin FM, metallic/spin A-type AFM; insulating/spin C-type AFM, and finally insulating/spin G-type for $x = 1$. So far we did not investigate the spin structures of the magnetic phases for $x \geq 1$. Theoretically, taking SE, DE and orbital degeneracy into account the sequence of spin structures A-F-A-C-G has been predicted.¹³ We want to stress that a pure insulating AFM state appears in all phase diagrams at high doping levels and that a G-type antiferromagnet is stable for $x = 1$. The spin structure close to $x = 0.8$ (AFM, C-type) has been taken in analogy to other doped manganites and to the existing literature. For this concentration regime around $x = 0.8$ evidence for charge order can be found due to the sharp increase of the resistivity at T_N , possibly in the form of stripe or bistrife structures as it has been suggested in literature.²¹ Close to $x = 0.6$ it has been proposed that the orbitals are strictly aligned within the a, b -plane forcing an A-type spin structure.¹³ $\text{La}_{0.4}\text{Sr}_{0.6}\text{MnO}_3$ reveals antiferromagnetic order with a FM component, which is of the order of $0.1 \mu_B$ at low fields. It is this concentration regime where also two-dimensional metallic behavior is expected.

In what follows we would like to compare the phase diagram of $\text{La}_{1-x}\text{Sr}_x\text{MnO}_3$ as observed in the present investigations with published phase diagrams of other manganites and with theoretical predictions. This discussion is based on experiments covering the hole and

electron doped regime of the phase diagram and investigating the half-doped case in detail. Experimental phase diagrams are available for La:Sr⁷, La:Ca³³, Pr:Sr^{13,14,30}, Pr:Ca^{14,34}, Nd:Sr^{13,30}, Sm:Sr and Sm:Ca¹⁴ manganite. From these results a generic electronic phase diagram can be deduced, which yields the sequence of AFM (A-type)/I, FM/I, FM/M and AFM/I (C-type). The latter spin structure dominates a broad region in the electron doped ($x > 0.5$) crystals. It is clear that these spin structures and electronic properties are closely linked with the orbital degrees of freedom, and the orbital order for most of these phases has been theoretically proposed by Maezono et al.¹³, Khomskii²², van den Brink et al.³⁵ and by Solov'yev and Terakura.³⁶

It is worth mentioning that there are some noticeable exceptions from this universal phase diagram: e.g. the Sm:Ca¹⁴ and the Pr:Ca^{14,34} compounds do not exhibit a typical CMR regime with a ferromagnetic and insulating ground state for $x < 0.5$. This fact probably results from geometrical constraints. In addition peculiarities show up close to half filling: In the Nd:Sr and Pr:Sr compounds close to $x = 0.5$ charge ordered antiferromagnetic phases were found.³⁰ Magnetically these systems form ferromagnetic zig-zag chains which are coupled antiferromagnetically. This CE-type of magnetic structure results from charge and orbital order and has been explained theoretically in detail.^{35,36} The FM zig-zag chains with their concomitant charge order can easily be molten by the application of moderate magnetic fields.³⁷ In addition, van den Brink et al.³⁵ have shown that for doping $x < 0.5$ the CE structure is unstable against phase separation. This CE-type spin structure with a checkerboard-type CO is not observed in the La:Sr compound under investigation. In our high-quality samples we find an AFM and metallic ground state with no signs of charge order. Hence we do not expect to find a CE-type magnetic structure. A metallic AFM spin A-type phase has been predicted by Maezono et al.¹³ which reveals an $(x^2 - y^2)$ orbital structure. In this structure hopping along c is forbidden and the metallic conductivity is strictly two dimensional and indeed this type of behavior has been observed in $\text{Nd}_{0.45}\text{Sr}_{0.55}\text{MnO}_3$.³² We believe that this type of spin and orbital structure may also be present in $\text{La}_{1-x}\text{Sr}_x\text{MnO}_3$ for $x \approx 0.6$. Measurements of the magnetic structure and of the anisotropy of the electronic transport still have to be performed. It remains a puzzle why in $\text{Nd}_{0.45}\text{Sr}_{0.55}\text{MnO}_3$, which reveals a metallic, spin A-type phase, Kuwahara et al.³² observed a significant anisotropy in the resistivity but not in the magnetic susceptibility. In contrast $\text{La}_{0.45}\text{Sr}_{0.55}\text{MnO}_3$ exhibits a pronounced anisotropy both in the FM and in the AFM states (cf. Fig. 6). It seems clear that the FM metallic state at elevated temperatures still is driven by double exchange, and perhaps the low-temperature metallic state indicates electronic phase separation where the FM metallic paths still percolate. The occurrence of a FM metal followed by an AFM metallic state for concentrations close to $x = 0.6$ still is a puzzle and further experi-

mental work is needed to elucidate this strange phase.

Acknowledgments

This work was supported by the Bundesministerium für Bildung und Forschung (BMBF) via VDI/EKM, FKZ

13N6917, by the Deutsche Forschungsgemeinschaft via SFB 484 (Augsburg), and by INTAS via project 97-30850.

-
- ¹ R. von Helmolt, J. Wecker, B. Holzapfel, L. Schultz, and K. Samwer, *Phys. Rev. Lett.* **71**, 2331 (1993); K. Chahara, T. Ohono, M. Kasai, Y. Kanke, and Y. Kozono, *Appl. Phys. Lett.* **62**, 780 (1993)
- ² E. Dagotto, T. Hotta, and A. Moreo, *Physics Reports* **344**, 1 (2001)
- ³ P.G. de Gennes, *Phys. Rev.* **118**, 141 (1960)
- ⁴ A.J. Millis, B.I. Shraiman, and R. Mueller, *Phys. Rev. Lett.* **77**, 175 (1996)
- ⁵ Y. Endoh, K. Hirota, S. Ishihara, S. Okamoto, Y. Murakami, A. Nishizawa, T. Fukuda, H. Kimura, H. Nojiri, K. Kaneko, and S. Maekawa, *Phys. Rev. Lett.* **82**, 4328 (1999)
- ⁶ M. Paraskevopoulos, F. Mayr, J. Hemberger, A. Loidl, R. Heichele, D. Maurer, V. Mueller, A.A. Muhkin, and A.M. Balbashov, *J. Phys.: Condens. Matter* **12**, 3993 (2000); M. Paraskevopoulos, F. Mayr, Ch. Hartinger, A. Pimenov, J. Hemberger, P. Lunkenheimer, A. Loidl, A.A. Muhkin, V.Yu. Ivanov, and A.M. Balbashov, *J. Magn. Magn. Mater.* **211**, 118 (2000)
- ⁷ T. Niemoeller, M. von Zimmermann, S. Uhlenbruck, O. Friedt, B. Büchner, T. Frello, N.H. Andersen, P. Berthet, L. Pinsard, A.M. de Leon-Guevara, A. Revcolevschi, and J.R. Schneider, *Eur. Phys. J.* **B8**, 5 (1999)
- ⁸ J.B. Goodenough and J.M. Longo, in "Landolt-Bornstein: New Series", Volume III/4, Springer Verlag, Berlin (1970), p.126 ff
- ⁹ A. Urushibara, Y. Moritomo, T. Arima, A. Asamitsu, G. Kido, and Y. Tokura, *Phys. Rev.* **B51**, 14103 (1995)
- ¹⁰ Y. Yamada, O. Hino, S. Nohdo, R. Kanao, T. Inami, and S. Katano, *Phys. Rev. Lett.* **77**, 904 (1996)
- ¹¹ H. Kawano, R. Kajimoto, M. Kubota, and H. Yoshizawa, *Phys. Rev.* **B53**, R14709 (1996)
- ¹² J.-S. Zhou, J.B. Goodenough, A. Asamitsu, and Y. Tokura, *Phys. Rev. Lett.* **79**, 3234 (1997)
- ¹³ R. Maezono, S. Ishihara, and N. Nagaosa, *Phys. Rev.* **B57**, 13993 (1998), *Phys. Rev.* **B58**, 11583 (1998), and references therein
- ¹⁴ C. Martin, A. Maignan, M. Hervieu, and B. Raveau, *Phys. Rev.* **B60**, 12191 (1999)
- ¹⁵ T. Akimoto, Y. Maruyama, Y. Moritomo, A. Nakamura, K. Hirota, K. Ohoyama, and M. Ohashi, *Phys. Rev.* **B57**, R5594 (1998)
- ¹⁶ Y. Moritomo, T. Akimoto, A. Nakamura, K. Ohoyama, and M. Ohashi, *Phys. Rev. B* **58**, 5544 (1998)
- ¹⁷ H. Fujishiro, T. Fukase, and M. Ikebe, *J. Phys. Soc. Jpn.* **67**, 2582 (1998)
- ¹⁸ S.I. Patil, S.M. Bhagat, Q.Q. Shu, S.E. Lofland, S.B. Ogale, V.N. Smolyaninova, X. Zhang, B.S. Palmer, R.S. Decca, F.A. Brown, H.D. Drew, R.L. Green, I.O. Troyanchuk, and W.H. McCarroll, *Phys. Rev.* **B62**, 9548 (2000)
- ¹⁹ A. Arrot and J.E. Noakes, *Phys. Rev. Lett.* **19**, 786 (1967)
- ²⁰ P.G. Radaelli, D.E. Cox, L. Capogna, S.-W. Cheong, and M. Marezio, *Phys. Rev.* **B59**, 14440 (1999)
- ²¹ S. Mori, C.H. Chen, and S.-W. Cheong, *Nature* **392**, 479 (1998) and *Phys. Rev. Lett.* **81**, 3972 (1998)
- ²² D.I. Khomskii, cond-mat/0104517 (2001); D.I. Khomskii and K.I. Kugel, *Europhys. Lett.* **55**, 208 (2001)
- ²³ K. Held and D. Vollhardt, *Phys. Rev. Lett.* **84**, 5168 (2000); K. Held and D. Vollhardt, *Eur. Phys. J.* **B5**, 473 (1998)
- ²⁴ J. van den Brink and D. Khomskii, *Phys. Rev. Lett.* **82**, 1016 (1999)
- ²⁵ For an overview of the different types of spin structures in perovskites the reader is referred to: J.B. Goodenough, *Magnetism and the Chemical Bond*, J. Wiley & Sons, New York, 1963, p. 94
- ²⁶ A.M. Balbashov, S.G. Karabashev, Ya.M. Mukovskiy, and S.A. Zverkov, *J. Crystal Growth* **167**, 365 (1996)
- ²⁷ A. Krimmel, J. Hemberger, A.A. Mukhin, A. Balbashov, and A. Loidl, to be published
- ²⁸ P.G. Radaelli, D.E. Cox, M. Marezio, and S.-W. Cheong, *Phys. Rev. B* **55**, 3015 (1997)
- ²⁹ M.R. Lees, J. Barratt, G. Balakrishnan, D.M. Paul, and C. Ritter, *Phys. Rev. B* **58**, 8694 (1998)
- ³⁰ H. Kawano, R. Kajimoto, H. Yoshizawa, Y. Tomioka, H. Kuwahara, and Y. Tokura, *Phys. Rev. Lett.* **78**, 4253 (1997)
- ³¹ M. Hervieu, G. Van Tendeloo, V. Caignaert, A. Maignan, and B. Raveau, *Phys. Rev. B* **53**, 14274 (1996)
- ³² H. Kuwahara, T. Okuda, Y. Tomioka, A. Asamitsu, and Y. Tokura, *Phys. Rev. Lett.* **82**, 4316 (1999)
- ³³ P. Schiffer, A.P. Ramirez, W. Bao, and S.-W. Cheong, *Phys. Rev. Lett.* **75**, 3336 (1995); A.P. Ramirez, P. Schiffer, S.-W. Cheong, C.H. Chen, W. Bao, T.T.M. Palstra, P.L. Gammel, D.J. Bishop, and B. Zegarski, *Phys. Rev. Lett.* **76**, 3188 (1996)
- ³⁴ Y. Tomioka, A. Asamitsu, H. Kuwahara, Y. Moritomo, and Y. Tokura, *Phys. Rev.* **B53**, R1689 (1996)
- ³⁵ J. van den Brink, G. Khaliullin, and D. Khomskii, *Phys. Rev. Lett.* **83**, 5118 (1999)
- ³⁶ I.V. Solov'yev and K. Terakura, *Phys. Rev. Lett.* **83**, 2825 (1999)
- ³⁷ H. Kuwahara, Y. Tomioka, A. Asamitsu, Y. Morimoto, and Y. Tokura, *Science* **270**, 961 (1995)